RSC Advances

PAPER

View Article Online
View Journal | View Issue

Cite this: *RSC Adv.*, 2022, **12**, 4874

Bimetallic docked covalent organic frameworks with high catalytic performance towards coupling/oxidation cascade reactions†

Yaling Li,‡[a] Kaiming Zuo,‡[a] Tingjun Gao,[a] Jifeng Wu,[a] Xiaofang Su,[a] Chaoyuan Zeng,*[a] Huanjun Xu,[ab] Hui Hu,[a] Xiaosong Zhang[c] and Yanan Gao *[a]

Received 10th July 2021
Accepted 2nd February 2022

DOI: 10.1039/d1ra05315a

rsc.li/rsc-advances

Covalent organic frameworks (COFs) are an emerging class of crystalline porous polymers that make these materials suitable for use as excellent scaffold in heterogeneous catalysis. Here we synthesize a layered two-dimensional (2D) COF (TADP–COF) through the condensation reaction between four-branched 5,10,15,20-tetrakis(4-aminophenyl)porphyrin (TAPP) and linear 2,5-dihydroxyterephthalaldehyde (Dha) and 1,4-phthalaldehyde (PA) building blocks. Porphyrin units, imine and hydroxyl groups together with imines can provide wide coordination sites for metal docking. Using a programmed synthetic procedure, Cu(II) ions first coordinated with the imine groups in conjunction with their adjacent hydroxyl groups, and porphyrin units and subsequently added Pd(II) ions occupied the remaining imine sites in the space between adjacent COF layers. The bimetallic Pd(II)/Cu(II)@TADP–COF showed high catalytic activity in a one-pot coupling/oxidation cascade reaction in water. The high surface area, one-dimensional (1D) open channel structure and predesigned catalytic active sites of this material make it ideal candidate for use as heterogeneous catalyst in a wide range of catalytic reactions.

1 Introduction

Covalent organic frameworks (COFs) are two-dimensional (2D) and three-dimensional (3D) crystalline porous polymers which are composed of light weight elements like B, C, H, N, O and so on.[1,2] COFs have attracted much attention in recent years because they have exhibited many important applications in various research areas, such as catalysis,[3–9] gas storage/separation,[10–16] sensing[17,18] and energy conversion.[19–24] COFs are constructed according to the principles of reticular chemistry, where building blocks with predesigned geometries and radicals are self-assembled together *via* reversible covalent bonds to produce extended periodic networks. The general features of this strategy allow for the flexible regulation of pore properties, including pore size, pore shape, volume, and distribution. Besides, it is possible for these COFs to introduce functional active species to the framework of the COFs. Therefore, these novel materials can be widely recognized as promising platforms for the immobilization of catalysts for use in organic synthesis.

2D COFs are relatively easier to synthesize than 3D COFs because it is accepted that 2D COFs are formed through the stacking of COF layers[25–27] and 2D COFs have therefore been explored in detail in terms of their application to catalysis.[4,28,29] The vertical alignment of COF layers through π–π interactions resulted in the formation of one-dimensional (1D) open channel structure, which not only significantly enhances the diffusion of substances, but can also be used to load catalysts through the post-synthetic modification of the COFs' skeleton.[28,30] Although earlier reported boronate ester-linked COFs are prone to decompose in air,[31,32] the recently developed triazine-type COFs[33] and Schiff-based COFs[34–36] exhibit greater stability towards high temperature, water, acid, base, and various organic solvents, making them quite amenable to standard catalytic conditions. 2D imine-linked COFs are successful to incorporate palladium ions or palladium nanoparticles and the Pd-loaded COFs have shown superior catalytic performances in C–C coupling reactions compared to conventional palladium catalysts.[4,37] Only negligible levels of catalyst leaching was observed, which can be ascribed to the strong coordination between imine ligands and metals. Because building blocks are arranged in a periodic lattice, imines are distributed uniformly throughout the framework of COFs, which allows for the effective isolation of the active species at a molecular level.[38] It is noteworthy that this level of uniform

[a]*Key Laboratory of Ministry of Education for Advanced Materials in Tropical Island Resources, Hainan University, No. 58, Renmin Avenue, Haikou 570228, China. E-mail: ygao@hainanu.edu.cn; zengchaoyuan@hainanu.edu.cn*

[b]*School of Science, Qiongtai Normal University, No. 8, Fuchengzhong Road, Haikou 571127, China*

[c]*Mechanical and Electrical College, Hainan University, No. 58, Renmin Avenue, Haikou 570228, China*

† Electronic supplementary information (ESI) available. See DOI: 10.1039/d1ra05315a

‡ Yaling Li and Kaiming Zuo should be considered as first authors.

dispersion is not easy to achieve for conventional catalyst supports.

It has been reported the usage of 2D imine-based COFs as heterogeneous catalyst carriers.[4,37,39,40] In these COFs, the imine was used to capture metal ions. For instance, Wang and his co-workers used COF–LZU1 to load Pd(II) to obtain a metal-doped COF catalyst, where Pd^{2+} ions were coordinated with imines within the space between adjacent COF layers.[4] In addition to Pd(II), Ni(II) and Cu(II) were also loaded into the COF skeleton through the coordination with imines in conjunction with their adjacent hydroxyl groups.[39,40] Recently, Zhao *et al.*[41] developed a supramolecular-based linkage engineering strategy to conduct a versatile 2D hydrazone-linked COF platform for the coordination of seven transition metal ions M(II) (M = Pd, Mn, Zn, Co, Ni, Cd and Cu). The bidentate coordination mode through the pyridine and hydrazone nitrogen atom in Pd/COF–DB endows it with high catalytic activity and recycling performance as a catalyst for the Suzuki–Miyaura cross-coupling reaction.[41] However, in many cases, it is necessary to dock different metals into a catalyst to achieve the purpose of catalysis. Over years, researchers have turned their attentions to study bimetallic catalysts because such catalysts can offer potentially increased activities, selectivities and enhanced stability when compared to their monometallic counterparts. For instance, our group designed and synthesized a series of 2D COFs containing two different nitrogen ligands to selectively coordinate Rh(II) and Pd(II) that showed excellent catalytic activity in one-pot addition–oxidation cascade reaction.[42] Subsequently, a Mn/Pd bimetallic docked COF has been developed and showed high catalytic activity in a Heck-epoxidation tandem reaction.[43]

As a continuation of our previous work, we report here the development of a similar procedure allowing for bimetallic docking in a different 2D COF using a pore surface engineering strategy. Through a three-component condensation reaction, hydroxyl groups were introduced into the skeleton of the 2D COF, which provides two different sorts of ligands, with one ligand (imine in conjunction with adjacent hydroxyl groups) favoring binding Cu(II) and the other ligand (only remaining imine) favoring binding Pd(II) in the space between adjacent COFs' layers. The selective coordination of imine ligands to the two different metal ions has been realized using a programmed synthetic procedure. The catalytic performance of the bimetallic COF has been investigated and the results indicated that the Pd(II)/Cu(II)@TADP–COF showed high catalytic activity in a one-pot coupling/oxidation cascade reaction. Among various solvents, water was found to be more efficient for the cascade reaction. The work described in this study is of significance that further confirmed that 2D COFs are a versatile platform for a range of heterogeneous catalytic reactions.

2 Experimental section

2.1. Synthesis of TADP–COF

5,10,15,20-Tetrakis(4-aminophenyl)porphyrin (TAPP) (27 mg, 0.04 mmol), 2,5-dihydroxyterephthalaldehyde (Dha) (6.6 mg, 0.04 mmol) and 1,4-phthalaldehyde (PA) (5.4 mg, 0.04 mmol) were placed in a glass ampule vessel (10 mL), followed by adding a solution of 1,2-dichlorobenzene (*o*-DCB)/*n*-butanol (1/1 by vol.; 2 mL). The mixture was sonicated for 5 min and the vessel was then flash frozen in liquid nitrogen. After that, 0.2 mL of 6.0 M acetic acid was rapidly added into the vessel. The reaction system was flash frozen in liquid nitrogen bath to degas by freeze–pump–thaw for three cycles. The internal pressure of the vessel was controlled below 5 Pa. The vessel was rapidly sealed with a flame, and then heated at 120 °C for 3 days. After the reaction, the COF powder was filtered out, washed with tetrahydrofuran (THF), *N*,*N*-dimethylformamide (DMF), and acetone and dried under vacuum at 120 °C for 10 h to give purple powder in 83% yield. The elemental analysis for TADP–COF was measured to be C 74.8%, N 11.9%, and H 5.1%, close to the theoretical values (C 79.8%, N 12.4%, and H 4.2%).

2.2. Synthesis of Cu(II)@TADP–COF

Copper acetate monohydrate (40 mg, 0.20 mmol) was dissolved in methanol (30 mL), and then TADP–COF (75 mg) was added. The mixture was stirred for 24 h at 50 °C. Then, the precipitate was washed with water and methanol thoroughly. The obtained Cu(II)@TADP–COF was then activated under vacuum overnight at 90 °C to give dark-purple powder in 91% yield.

2.3. Synthesis of Pd(II)@TADP–COF

Palladium acetate (44.9 mg, 0.20 mmol) was dissolved in dichloromethane (30 mL), and then TADP–COF (75 mg) was added. The mixture was stirred for 24 h at room temperature. After that, the precipitate was washed with water and methanol thoroughly. The obtained Pd(II)@TADP–COF was then activated under vacuum overnight at 90 °C to give dark-purple powder in 94% yield.

2.4. Synthesis of Pd(II)/Cu(II)@TADP–COF

60 mg of freshly prepared Cu(II)@TADP–COF was treated with 20 mg palladium acetate dissolved in 20 mL of dried dichloromethane. The mixture was stirred for 24 h at room temperature. The precipitate was collected by filtration and washed several times with dichloromethane, then dried under vacuum to give dark-purple Pd(II)/Cu(II)@TADP–COF powder in 93% yield.

2.5. Characterization

Fourier transform infrared (FT-IR) spectra were recorded in the region of 4000–400 cm^{-1} with KBr pellet method on a Bruker spectrophotometer (model TENSOR 27). The metal contents were measured by inductively coupled plasma optical emission spectroscopy (ICP-OES) through ICP-OES 7300DV (PerkinElmer). After calcination of sample at 1000 °C for 12 h, the residue was dissolved by aqua regia and diluted with water to prepare a solution for testing. X-ray photoelectron spectroscopy (XPS) measurement was performed with a ESCALAB 250Xi analyser, equipped with Al Kα radiation (1486.6 eV, 200 W). All power X-ray diffraction (PXRD) measurements were recorded in the 2θ range of 2.5–30° using a PANalytical X'Pert model Pro Multipurpose Diffractometer using Cu Kα radiation at 40 kV

and 40 mA. The signals were collected at 0.03° step scan with exposure time of 10 s per step. N_2 gas sorption isotherms were measured volumetrically at 77 K using a Quantachrome Autosorb-iQ2 analyzer. The sample was first activated at 100 °C for 15 h under high vacuum before analysis. Brunauer–Emmett–Teller (BET) model was used to determine the specific surface areas using desorption branches over P/P_0 of 0.01–0.05. The nonlocal density functional theory (NLDFT) method was used to evaluate the pore size distribution. Thermogravimetric analysis (TGA, STA449F3, NETZSCH, Germany) was carried out from room temperature to 600 °C. The heating rate is 10 °C min^{-1} and a N_2 flow rate of 20 mL min^{-1} was used. The reaction products were analyzed by on-line gas chromatography (Agilent 7890A) equipped with a capillary column (HP-5, 30 m × 0.25 mm) using a flame ionization detector. ^1H nuclear magnetic resonance (NMR) spectra were recorded by a Bruker Advance III 400 MHz NMR spectrometer (Bruker BioSpin Corporation, Fällanden, Switzerland) using tetramethylsilane as internal reference.

2.6. General procedures for one-pot coupling/oxidation cascade reaction

In a typical experiment, the reaction was performed using 4 mg of Pd(II)/Cu(II)@TADP–COF as catalyst in the presence of 4-iodobenzylic alcohol (0.2 mmol), phenylboronic acid (0.3 mmol), triethylamine (3.0 equiv.), TEMPO (0.25 equiv.) and H_2O (1.0 mL) at 60 °C for 6 h under a nitrogen atmosphere. After that, the internal N_2 was purged with O_2 using a balloon and the reaction was kept at 80 °C for another 15 h. The conversion and the yield of the products were analyzed by flame ionization gas chromatography (GC) using a capillary column (TC-FFAP). After the reaction, tridecane was added to the reaction solution as an internal standard. The mixture was filtered, and the solid was washed with methanol and vacuum overnight at 90 °C for recycle using.

3 Results and discussion

3.1. Synthesis and characterization of COFs

The construction of TADP–COF was based on a previous report by Banerjee *et al.* where the introduction of hydroxyl groups in building block enhanced the crystallinity and stability of DhaTph COF.[44] Here, we construct a similar COF, *i.e.*, TADP–COF, through the condensation reaction between four-branched TAPP and linear Dha and PA building blocks (Scheme 1). Different from the work reported by Banerjee group, PA was also used as edges to construct COF together with Dha. Three-component condensation reaction has been widely used to construct functional COFs, in which functional sites can be integrated into the skeleton of COFs through using desired functional building units. The molar ratio of Dha/PA is actually controllable, which means that the three-component condensation reaction allows for the precise control of the content of Cu(II) and Pd(II) in the TADP–COF. However, for simplify, the molar ratio of Dha/PA was set at 1 : 1 in this work.

The formation of TADP–COF was confirmed by Fourier transform infrared (FT-IR) spectrum. It can be seen from Fig. 1 that the reactants were remarkably consumed, as evidenced by the disappearance of the characteristic –N–H– (3286–3372 cm^{-1}) and –CHO– (1663 cm^{-1}) stretching bands. Meanwhile, the appearance of the characteristic stretching bands at 1605 cm^{-1} can be ascribed to the formation of imine bonds. This indicated the successful formation of imine-linked COF through the condensation of TAPP and Dha/PA under solvothermal condition.

The crystalline nature of TADP–COF was analyzed by powder X-ray diffraction (PXRD) measurements in combination with theoretical simulation. TADP–COF exhibited strong diffraction peaks at 3.4°, 6.9° and 23.5°, which can be attributed to the (100), (200) and (001) facets, respectively (Fig. 2a, black curve). The use of lattice modelling and Pawley refinement processes

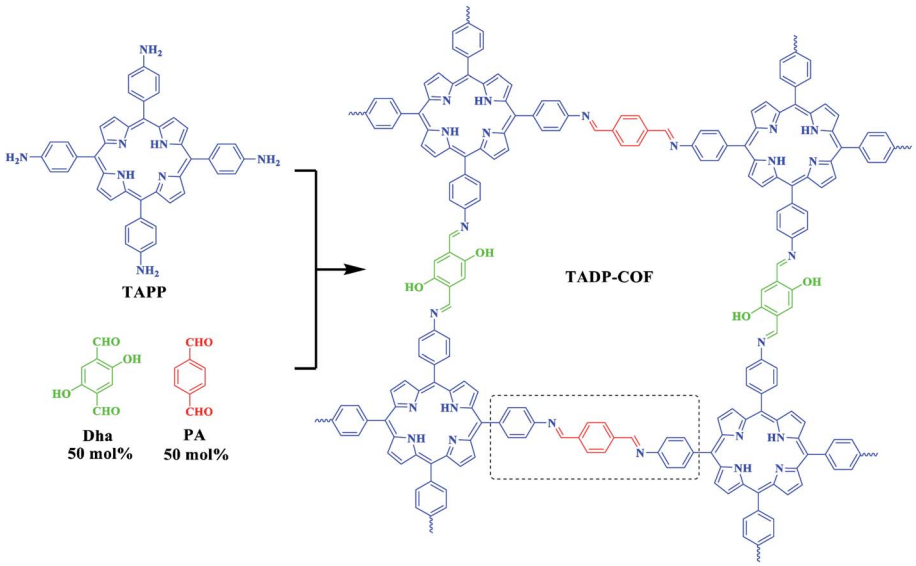

Scheme 1 Synthesis of TADP–COF.

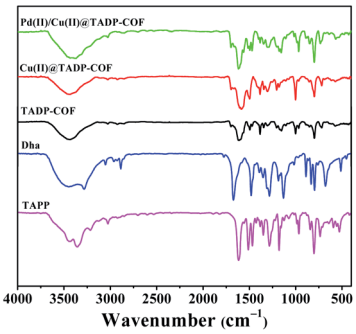

Fig. 1 FT-IR spectra of Dha, TAPP, TADP–COF, Cu(II)@TADP–COF and Pd(II)/Cu(II)@TADP–COF.

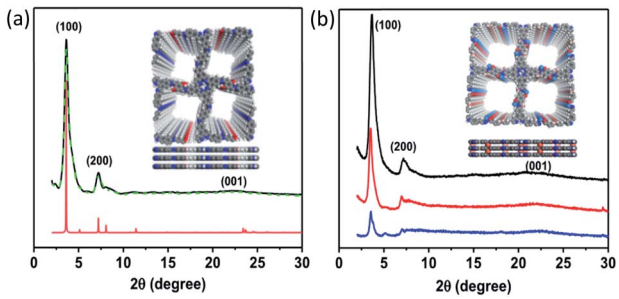

Fig. 2 (a) PXRD pattern of TADP–COF. Observed PXRD pattern (black), refined modelling profile (green) and simulated PXRD pattern (red) for an eclipsed AA stacking structure (red); (b) comparison of PXRD patterns of TADP–COF (black), Cu(II)@TADP–COF (red) and Pd(II)/Cu(II)@TADP–COF (blue).

led to an eclipsed AA stacking model that could reproduce the PXRD results with regards to the peak position and intensity (Fig. 2a, red curve). The Pawley refinement (Fig. 2a, green curve) using a unit cell of $\alpha = \gamma = 90°$, $\beta = 88.92°$, $a = c = 24.52$ Å, and $b = 3.79$ Å confirmed the peak assignment. The pseudo-Voigt function was used for whole profile fitting, and the Berar–Baldinozzi method was used for asymmetry correction during the refinement processes. The final R_{wp} and R_p values were 3.67% and 1.83%, respectively, for the TADP–COF. The PXRD pattern of TADP–COF was found to be similar with that of DhaTph COF,[44] suggesting that both COFs possess a similar arrangement structure. This result is in accordance with the previous observation that the introduction of a functional structural analogue of edge units into 2D COFs usually does not change their original topological structure.[45–47] There are actually two possible inter layer stacking models for Dha and PA in the skeleton of the COF, *i.e.*, model 1: Dha on top of Dha and PA on top of PA and model 2: Dha on top of PA and PA on top of Dha between the layers. However, our theoretical calculations using DFTB method revealed that the energy of the model 1 is −91.2 kcal mol^{-1} lower than that of model 2 (see ESI†), suggesting that model 1 is more reasonable. Even so, here we do not exclude the possibility that a disordered arrangement may coexist with our proposed structure. After loading Cu(II) and Pd(II) to the COF successively, the position of diffraction peaks was not changed (Fig. 2b), indicating that the topological structure of maternal TADP–COF remained. But the crystallinity of Cu(II)@TADP–COF and Pd(II)/Cu(II)@TADP–COF was lower than that of their maternal TADP–COF.

As mentioned above, a programmed synthetic procedure was carried out to realize the bimetallic loading (Scheme 2). It has been reported that $Pd(OAc)_2$ can coordinate with nitrogen atoms of imines between the adjacent layers of imine-linked COFs.[4,42,43] However, Cu^{2+} can only coordinate with nitrogen atoms of imines between the adjacent layers in conjunction with their two adjacent hydroxyl groups in the form of tetrahedral coordination in the framework.[40] Considering these facts, we first docked $Cu(OAc)_2$ to the TADP–COF to obtain Cu(II)@TADP–COF and then loading of $Pd(OAc)_2$ was subsequently performed to produce Pd(II)/Cu(II)@TADP–COF. Porphyrins are known to be good ligands to load various metals, and thus we do not exclude the possibility that Cu^{2+} or Pd^{2+} was coordinated within the porphyrins of TADP–COF when $Cu(OAc)_2$ or $Pd(OAc)_2$ was added.

The Cu content in the Cu(II)@TADP–COF was measured by inductively coupled plasma optical emission spectroscopy (ICP-OES) to be 9.7 wt%, which is less than the theoretical value of 12.4 wt% (ESI†), if supposing that Cu^{2+} was coordinated with both porphyrin units and nitrogen atoms of imines in conjunction with two adjacent hydroxyl groups. Considering the possible defects of crystalline COFs, the coordination of Cu^{2+} with porphyrin and imine ligands should be quite complete. After subsequent loading Pd(II) into the Cu(II)@TADP–COF, the Cu content of Pd(II)/Cu(II)@TADP–COF was 7.3 wt%, lower than the theoretical value of 10.2 wt% (ESI†), suggesting that a little amount of Cu(II) may be replaced by Pd(II) after Pd(II) was subsequently added.[41] The Pd content in the Pd(II)/Cu(II)@TADP–COF was determined to be 7.4 wt%, which is close to the theoretical value of 8.4 wt% (ESI†). This result reveals that Pd(II) was mainly coordinated with the remaining imine groups. To confirm our assumption, we prepared a TAPP–PA–COF that was constructed through the condensation reaction of TAPP and PA (ESI†). This means that no phenolic hydroxyl appeared in the skeleton of the COF and Pd(II) would coordinate with all the imines and porphyrins in the COF. When $Cu(OAc)_2$ was added to the TAPP–PA–COF, the Cu content in the COF was 6.2 wt%, close to the theoretical value of 6.9 wt% (supposed Cu is only docked by porphyrins, ESI†), indicating that Cu was only coordinated with porphyrin of the COF. Similarly, when $Pd(OAc)_2$ was added to the TAPP–PA–COF, the Pd content in the Pd(II)@TAPP–PA–COF was measured to be 19.7 wt%, which is close to the theoretical value of 22.3 wt% (supposed Pd is docked by porphyrins and all imines, ESI†). This result provides an indirect proof that Cu can be only coordinated with imines in the presence of phenolic hydroxyl group and Pd was then coordinated with the remaining imines. To further explore the coordination interaction between metals and TADP–COF, X-ray photoelectron spectroscopy (XPS) are performed (Fig. 3). The N 1s XPS spectrum of TADP–COF was deconvoluted into three typical bands at 398.1, 399.2, and 400.1 eV, which can be attributed to the binding energy of imine (–N=C–) linkage,[48] –NH– of porphyrins and –N=C– of

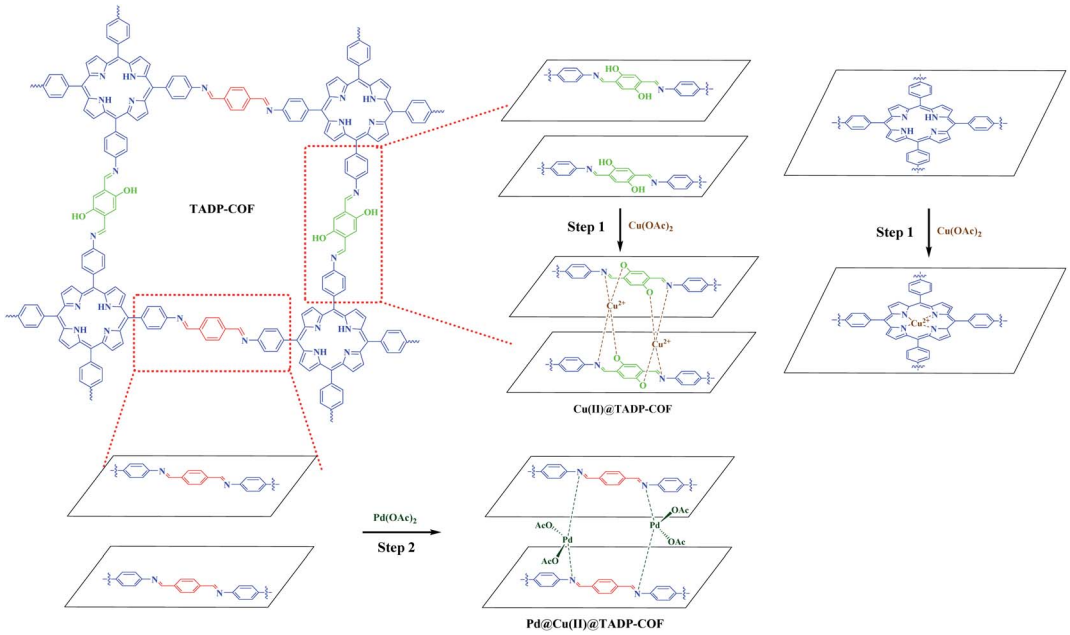

Scheme 2 Bimetallic loading of Cu(II) and Pd(II) using a programmed synthetic procedure.

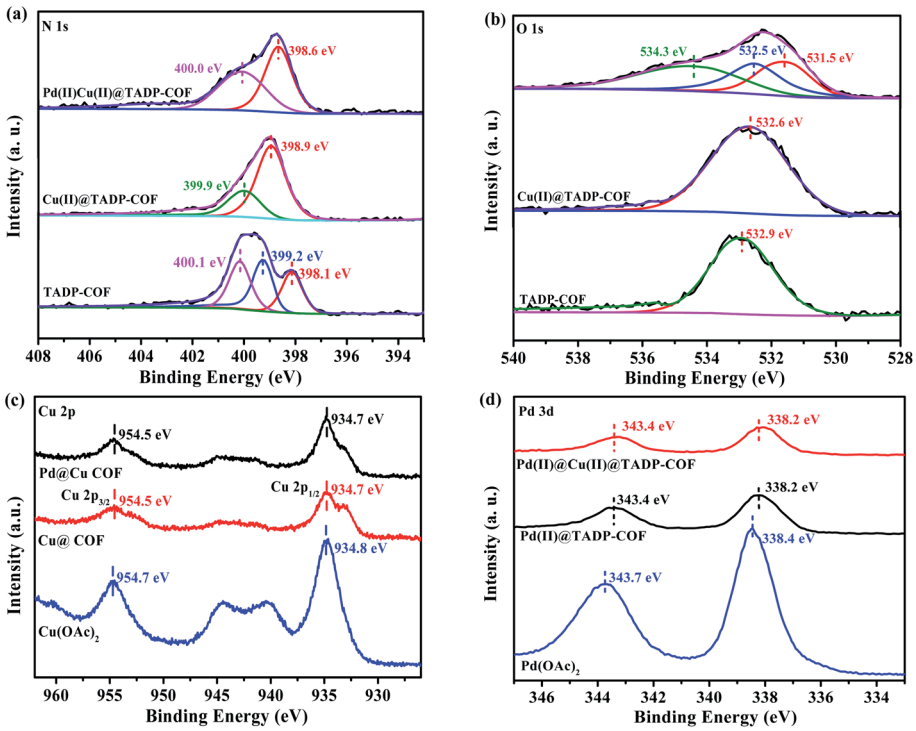

Fig. 3 XPS spectra of different COF samples: (a) N 1s, (b) O 1s, (c) Cu 2p and (d) Pd 3d.

porphyrins of the COF[49] (Fig. 3a). After loading Cu(II) into the TADP–COF, the N 1s peak at 398.1 eV was shifted upfield, and merged with the peak at 399.2 eV to appear at 398.9 eV as a broad peak. The peak at 399.9 eV can be ascribed to the binding energy of all the nitrogen atoms of porphyrins. We consider that the coordination of Cu(II) within the porphyrins produces a conjugate structure, which makes –NH– and –N=C– of porphyrins have the same environment. After successively adding Pd(II) to the Cu(II)@TADP–COF, the peak at 398.6 eV is due to the binding energy of metal-coordinated (both Cu and Pd) imines. Another peak at 400.0 eV originates from the conjugated nitrogen atoms of the porphyrins of the COF. The

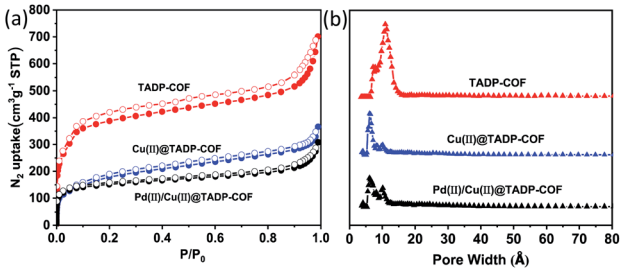

Fig. 4 N_2 adsorption–desorption isotherms (a) and their pose size distribution (b) of TADP–COF, Cu(II)@TADP–COF and Pd(II)/Cu(II) @TADP–COF recorded at 77 K, respectively.

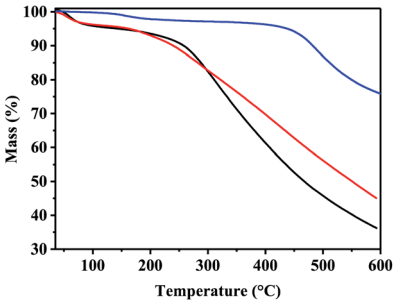

Fig. 5 TGA curves of TADP–COF (blue), Cu(II)@TADP–COF (red) and Pd(II)/Cu(II)@TADP–COF (black).

selective binding of Cu and Pd can also be proved by O 1s XPS spectrum (Fig. 3b). The binging energy at 532.9 eV is the O 1s signal of –OH of TADP–COF. When $Cu(OAc)_2$ was added, the signal shifted downfield to 532.6 eV, which can be ascribed to the replace of H^+ by Cu^{2+}. With further addition of $Pd(OAc)_2$, the O 1s signal was deconvoluted into three bands at 531.5, 532.5, and 534.3 eV. The peaks at 531.5 and 534.3 eV is the O 1s signals of acetate of $Pd(OAc)_2$ and the peak at 532.5 eV is the O 1s signal of –OCu. The coordination of Cu(II) and Pd(II) within the TADP–COF can also be confirmed by Cu 2p and Pd 3d XPS spectra. The shift downfield of Cu 2p signal can be observed after $Cu(OAc)_2$ was added to TADP–COF (Fig. 3c). A similar shift downfield was also found by $Pd(OAc)_2$ (Fig. 3d).[50,51] The shift downfield of both Cu 2p and Pd 3d signals can be attributed to the donor–acceptor interaction occurring through the coordination bonds between metal ions and the COF.[52] Considering that the catalyst was dried before, it is likely that a little amount of Cu with different valence state, like Cu(I) and Cu(0) was produced that participated in the catalysis.

The porous properties of all the COFs were characterized by nitrogen adsorption–desorption isotherms measured at 77 K. All the three COFs exhibited the typical type-I adsorption isotherms (Fig. 4a), indicative of microporous characteristics. The BET surface areas were measured to be 1234, 700 and 486 $m^2\ g^{-1}$, and the pore widths were calculated to be 1.1, 0.7 and 0.7 nm for the TADP–COF, Cu(II)@TADP–COF, and Pd(II)/Cu(II) @TADP–COF, respectively (Fig. 4b). Their corresponding total pore volumes were calculated to be 1.14, 0.45 and 0.40 $cm^3\ g^{-1}$, respectively (Table 1).

The thermal stability of the three COFs was further characterized by thermogravimetric analysis (TGA). It is clear from (Fig. 5) that TADP–COF decomposed at temperature above 400 °C, indicating its good thermal stability. A slight decrease in the curve was also observed at 100 °C, which may be due to the adsorbed small molecules like water or organic solvents. The thermal stability of Cu(II)@TADP–COF and Pd(II)/Cu(II)@TADP–COF is lower than that of TADP–COF, as reflected by their bigger weight loss. Similar to TADP–COF, the first weight loss at about 100 °C for Cu(II)@TADP–COF and Pd(II)/Cu(II)@TADP–COF can be ascribed to the lost water or organic solvents. The gradual weight loss after 100 °C may arise from the decreased crystal structure or decomposition of organic moiety of loaded metallic compounds. Therefore, it is practicable for reactions happened under 100 °C catalyzed by Pd(II)/Cu(II)@TADP–COF.

Table 1 Porous properties of TADP–COF, Cu(II)@TADP–COF and Pd(II)/Cu(II)@TADP–COF

COFs	S_{BET} ($m^2\ g^{-1}$)	Pore width (nm)	Total pore volume ($cm^3\ g^{-1}$)
TADP–COF	1234	1.1	1.14
Cu(II)@TADP–COF	700	0.7	0.45
Pd(II)/Cu(II)@TADP–COF	486	0.7	0.40

3.2. Catalytic performance of COFs

To evaluate the catalytic performance of the bimetallic COF, Pd(II)/Cu(II)@TADP–COF was used as catalysts for a cascade reaction. It is known that Pd-catalyzed Suzuki coupling of aryl halides and phenylboronic acid can produce bi-phenyl compounds in high yield.[53–55] On the other hand, benzyl alcohol can be oxidized to generate benzaldehyde under Cu(II) catalysis.[56,57] Thus, a cascade reaction consisting of the coupling reaction of 4-iodobenzyl alcohol and phenylboronic acid and then the oxidation reaction of intermediate [1,1′-biphenyl]-4-methanol to 4-biphenylcarboxaldehyde was chosen as a model reaction. It is anticipated that the separated loading of Cu(II) and Pd(II) gives bimetallic catalyst that can be used to catalyze this cascade reaction (Table 2).

A suitable reaction condition is of crucial importance in a cascade reaction, therefore we first screened the reaction conditions in the Suzuki coupling/oxidation cascade reaction. Acetonitrile, DMF and water were respectively used as solvent and reaction time was controlled at 6 h for the first step Suzuki coupling and 15 h for the next oxidation reaction. In these reactions, K_2CO_3 was used as a base. The yield of 4-biphenylcarboxaldehyde is only 34%, 41% and 54%, respectively (Table 2, entry 1–3). However, when an organic triethylamine (TEA) was used to substitute for K_2CO_3, the product yield increased to 91% in water (Table 2, entry 4). This reveals that water is an ideal solvent for this cascade reaction. When reaction time of the oxidation reaction was shortened to 5 h, a 51% yield (Table 2, entry 5) was observed, but the yield increased up to 85% when the reaction time of the oxidation reaction was

Table 2 Optimization of reaction conditions for the model reaction[a]

Entry	Catalysts	Time (h) [t_1 + t_2]	Solvent	Base	Yield[b] (%)
1	Pd(II)/Cu(II)@TADP–COF	6 + 15	CH_3CN	K_2CO_3	34
2	Pd(II)/Cu(II)@TADP–COF	6 + 15	DMF	K_2CO_3	41
3	Pd(II)/Cu(II)@TADP–COF	6 + 15	H_2O	K_2CO_3	54
4	Pd(II)/Cu(II)@TADP–COF	6 + 15	H_2O	TEA	91
5	Pd(II)/Cu(II)@TADP–COF	6 + 5	H_2O	TEA	51
6	Pd(II)/Cu(II)@TADP–COF	6 + 10	H_2O	TEA	85
7	Cu(II)@TADP–COF	6 + 15	H_2O	TEA	0
8	Pd(II)@TADP–COF	6 + 15	H_2O	TEA	8

[a] Reactions conditions: a mixture of 4-iodobenzyl alcohol (0.2 mmol), phenylboronic acid (1.5 equiv.), base (3.0 equiv.), TEMPO (0.25 equiv.), H_2O (2.0 mL), catalyst (4 mg) was stirred at 60 °C under N_2 (1.0 atm) for 6 h, and then O_2 atmosphere (balloon pressure) was introduced and the reaction continued at 80 °C for another 15 h. [b] Determined by GC using tridecane as an internal standard.

10 h (Table 2, entry 6). When Cu(II)@TADP–COF was used as catalyst, no product was obtained (Table 2, entry 7), while a low yield of 8% was obtained in the presence of Pd(II)@TADP–COF (Table 2, entry 8). Based on the above results, the following reaction condition was applied, *i.e.*, reaction time of 6 h for the first coupling at 60 °C, and 15 h for the next oxidation reaction at 80 °C in the presence of 2,2,6,6-tetramethylpiperidine-1-oxyl (TEMPO), TEA, and Pd(II)/Cu(II)@TADP–COF catalyst.

To illuminate the respective functions of Cu(II) and Pd(II) in this cascade reaction, the catalytic performance of Pd(II)/Cu(II)@TADP–COF for the separated reaction was investigated. The Suzuki coupling of 4-iodobenzyl alcohol and phenylboronic acid produced [1,1′-biphenyl]-4-methanol in 94% yield, and the oxidation of [1,1′-biphenyl]-4-methanol presented final product of 4-biphenylcarboxaldehyde in 97% yield. We also found that monometallic Pd(II)@TADP–COF can efficiently catalyze the Suzuki coupling (91% yield) but failed for the oxidation reaction because no oxidation product was obtained. Similarly, monometallic Cu(II)@TADP–COF was highly effective for the oxidation of [1,1′-biphenyl]-4-methanol (99% yield), but the yield of [1,1′-biphenyl]-4-methanol in the Suzuki coupling reaction was only 4%. This indicates that Pd(II) first catalyzed the Suzuki coupling of 4-iodobenzyl alcohol and phenylboronic acid to produce [1,1′-biphenyl]-4-methanol, which was then oxidized to give 4-biphenylcarboxaldehyde catalyzed by Cu(II). We then used a mixture of Cu(II)@TADP–COF and Pd(II)@TADP–COF as catalyst, in which the molar ration of Pd/Cu was controlled at 1 : 1.6 that is similar to Pd(II)/Cu(II)@TADP–COF. The yield of 4-biphenylcarboxaldehyde was only 83% when the mixed catalyst was used. Considering that the yield of 4-biphenylcarboxaldehyde was 91% when Pd(II)/Cu(II)@TADP–COF was used, this result indicates that a synergistic effect was observed for the reaction. Based on the above results, it is clear that the Pd(II)/Cu(II)@TADP–COF exhibited good catalytic activity towards the Suzuki coupling/oxidation cascade reaction. We assume that the large special surface area, 1D open channels and separated active sites of the catalyst contributed to its excellent catalytic performance.

In addition, the general applicability of the catalyst is of great importance for evaluating its catalyst performance. Under the optimized reaction conditions, the scope of the approach was focused. Table 3 shows the scope of various substrates for the coupling/oxidation cascade reaction. As expected, the reactions related to more active 4-iodobenzyl alcohol gave higher product yields than 4-bromobenzyl alcohol. Substituted phenylboronic acid with a weaker electron-rich methoxy group exhibited no clear effect on the cascade reaction (entry 2 and 5). However, this effect is evident for a strong electron withdrawing nitro group (entry 3 and 6). The stability and reusability of the Pd(II)/

Table 3 Catalytic performance of Pd(II)/Cu(II)@TADP–COF in the coupling/oxidation cascade reaction

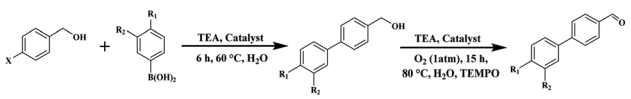

Entry	Substrate			Yield
1	X = I	R_1 = H	R_2 = H	91%
2	X = I	R_1 = OCH_3	R_2 = H	88%
3	X = I	R_1 = H	R_2 = NO_2	68%
4	X = Br	R_1 = H	R_2 = H	82%
5	X = Br	R_1 = OCH_3	R_2 = H	75%
6	X = Br	R_1 = H	R_2 = NO_2	37%

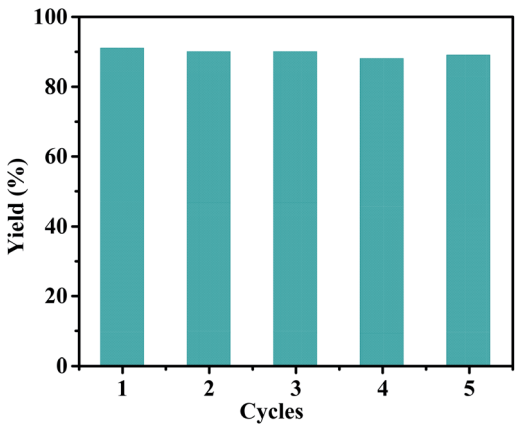

Fig. 6 Recyclability of the Pd(II)/Cu(II)@TADP–COF catalyst.

Cu(II)@TADP–COF were also investigated for the model reaction. As shown in (Fig. 6), the Pd(II)/Cu(II)@TADP–COF catalyst can be reused at least 5 times without apparently losing its catalytic activity and yield. ICP analysis revealed that neither Pd nor Cu is detectable in the filtrate after each cycle, suggesting that both metals are steadily incorporated with the skeleton of the TADP–COF.

4 Conclusions

In summary, an imine-linked two-dimensional (2D) COF with two different metallic coordination sites was designed and synthesized using a three-component system. Selective loading Cu(II) and Pd(II) into the COF was realized through a programmed synthetic procedure. Cu(II) was first coordinated with imines in conjunction with their adjacent hydroxyl groups and porphyrins of the COF and Pd(II) was subsequently coordinated with the remaining imines. The bimetallic Pd(II)/Cu(II)@TADP–COF exhibited good catalytic activity towards a one-pot Suzuki coupling/oxidation cascade reaction in water. Moreover, good stability and reusability of the COF were also observed. We image that this strategy would be extended to more bimetallic systems in catalyzing other sorts of cascade reactions and we expect that synergistic effects will be achieved to enhance the selectivity and activity of reactions using bimetallic COFs as catalysts.

Author contributions

Conceptualization, Y. L., T. G., C. Z. and Y. G.; methodology, Y. L., K. Z., T. G., J. W. and X. S.; software, H. H.; validation, H. X. and X. Z.; formal analysis, C. Z.; investigation, Y. L., K. Z. and J. W.; resources, X. H. and Y. G.; writing—original draft preparation, Y. L. and C. Z.; writing—review and editing, Y. G.; supervision, Y. G. All authors have read and agreed to the published version of the manuscript.

Conflicts of interest

The authors declare no conflict of interest.

Acknowledgements

This work was supported by the National Natural Science Foundation of China (21965011 and 21473196) and Natural Science Foundation of Hainan Province (2019RC110 and 2019RC250).

Notes and references

1 K. Geng, T. He, R. Liu, K. Tan, Z. Li, S. Tao, Y. Gong, Q. Jiang and D. Jiang, *Chem. Rev.*, 2020, **120**, 8814–8933.
2 X. Chen, K. Geng, R. Liu, K. Tan, Y. Gong, Z. Li, S. Tao, Q. Jiang and D. Jiang, *Angew. Chem., Int. Ed.*, 2020, **59**, 5050–5091.
3 S. Lin, C. S. Diercks, Y. Zhang, N. Kornienko, E. M. Nichols, Y. Zhao, A. R. Paris, D. Kim, P. Yang, O. M. Yaghi and C. Chang, *Science*, 2015, **349**, 1208–1213.
4 S. Ding, J. Gao, Q. Wang, Y. Zhang, W. Song, C. Su and W. Wang, *J. Am. Chem. Soc.*, 2011, **133**, 19816–19822.
5 V. S. Vyas, F. Haase, L. Stegbauer, G. Savasci, F. Podjaski, C. Ochsenfeld and B. V. Lotsch, *Nat. Commun.*, 2015, **6**, 1–9.
6 Q. Sun, B. Aguila, J. Perman, N. Nguyen and S. Ma, *J. Am. Chem. Soc.*, 2016, **138**, 15790–15796.
7 X. Wang, X. Han, J. Zhang, X. Wu, Y. Liu and Y. Cui, *J. Am. Chem. Soc.*, 2016, **138**, 12332–12335.
8 J. Zhang, X. Han, X. Wu, Y. Liu and Y. Cui, *J. Am. Chem. Soc.*, 2017, **139**, 8277–8285.
9 H. Xu, S. Ding, W. An, H. Wu and W. Wang, *J. Am. Chem. Soc.*, 2016, **138**, 11489–11492.
10 Y. Du, H. Yang, J. M. Whiteley, S. Wan, Y. Jin, S. H. Lee and W. Zhang, *Angew. Chem., Int. Ed.*, 2016, **55**, 1737–1741.
11 Y. Zeng, R. Zou and Y. Zhao, *Adv. Mater.*, 2016, **28**, 2855–2873.
12 L. A. Baldwin, J. W. Crowe, D. A. Pyles and P. L. McGrier, *J. Am. Chem. Soc.*, 2016, **138**, 15134–15137.
13 Y. Pramudya and J. L. Mendoza-Cortes, *J. Am. Chem. Soc.*, 2016, **138**, 15204–15213.
14 H. Furukawa and O. M. Yaghi, *J. Am. Chem. Soc.*, 2009, **131**, 8875–8883.
15 N. Huang, X. Chen, R. Krishna and D. Jiang, *Angew. Chem., Int. Ed.*, 2015, **54**, 2986–2990.
16 N. Huang, R. Krishna and D. Jiang, *J. Am. Chem. Soc.*, 2015, **137**, 7079–7082.
17 S. Dalapati, S. Jin, J. Gao, Y. Xu, A. Nagai and D. Jiang, *J. Am. Chem. Soc.*, 2013, **135**, 17310–17313.
18 J. Zhang, L. Wang, N. Li, J. Liu, W. Zhang, Z. Zhang, N. Zhou and X. Zhu, *CrystEngComm*, 2014, **16**, 6547–6551.
19 S. Wan, J. Guo, J. Kim, H. Ihee and D. Jiang, *Angew. Chem., Int. Ed.*, 2008, **47**, 8826–8830.
20 S. Wan, J. Guo, J. Kim, H. Ihee and D. Jiang, *Angew. Chem., Int. Ed.*, 2009, **48**, 5439–5442.
21 E. L. Spitler, J. W. Colson, F. J. Uribe-Romo, A. R. Woll, M. R. Giovino, A. Saldivar and W. R. Dichtel, *Angew. Chem., Int. Ed.*, 2012, **51**, 2623–2627.
22 M. Dogru, M. Handloser, F. Auras, T. Kunz, D. Medina, A. Hartschuh, P. Knochel and T. Bein, *Angew. Chem., Int. Ed.*, 2013, **52**, 2920–2924.
23 L. Chen, K. Furukawa, J. Gao, A. Nagai, T. Nakamura, Y. Dong and D. Jiang, *J. Am. Chem. Soc.*, 2014, **136**, 9806–9809.
24 C. R. DeBlase, K. E. Silberstein, T. T. Truong, H. D. Abruña and W. R. Dichtel, *J. Am. Chem. Soc.*, 2013, **135**, 16821–16824.
25 B. P. Biswal, S. Chandra, S. Kandambeth, B. Lukose, T. Heine and R. Banerjee, *J. Am. Chem. Soc.*, 2013, **135**, 5328–5331.
26 J. W. Colson, A. R. Woll, A. Mukherjee, M. P. Levendorf, E. L. Spitler, V. B. Shields, M. G. Spencer, J. Park and W. R. Dichtel, *Science*, 2011, **332**, 228–231.
27 X. Liu, C. Guan, S. Ding, W. Wang, H. Yan, D. Wang and L. Wan, *J. Am. Chem. Soc.*, 2013, **135**, 10470–10474.
28 H. Xu, X. Chen, J. Gao, J. Lin, M. Addicoat, S. Irle and D. Jiang, *Chem. Commun.*, 2014, **50**, 1292–1294.

29 A. P. Côté, A. I. Benin, N. W. Ockwig, M. O'Keeffe, A. J. Matzger and O. M. Yaghi, *Science*, 2005, **310**, 1166–1170.
30 X. Chen, N. Huang, J. Gao, H. Xu, F. Xu and D. Jiang, *Chem. Commun.*, 2014, **50**, 6161–6163.
31 A. P. Côté, H. M. El-Kaderi, H. Furukawa, J. R. Hunt and O. M. Yaghi, *J. Am. Chem. Soc.*, 2007, **129**, 12914–12915.
32 L. M. Lanni, R. W. Tilford, M. Bharathy and J. J. Lavigne, *J. Am. Chem. Soc.*, 2011, **133**, 13975–13983.
33 P. Kuhn, M. Antonietti and A. Thomas, *Angew. Chem., Int. Ed.*, 2008, **47**, 3450–3453.
34 F. J. Uribe-Romo, J. R. Hunt, H. Furukawa, C. Klöck, M. O'Keeffe and O. M. Yaghi, *J. Am. Chem. Soc.*, 2009, **131**, 4570–4571.
35 F. J. Uribe-Romo, C. J. Doonan, H. Furukawa, K. Oisaki and O. M. Yaghi, *J. Am. Chem. Soc.*, 2011, **133**, 11478–11481.
36 S. Kandambeth, A. Mallick, B. Lukose, M. V. Mane, T. Heine and R. Banerjee, *J. Am. Chem. Soc.*, 2012, **134**, 19524–19527.
37 P. Pachfule, M. K. Panda, S. Kandambeth, S. M. Shivaprasad, D. D. Diaz and R. Banerjee, *J. Mater. Chem. A*, 2014, **2**, 7944–7952.
38 L. Chen, S. Rangan, J. Li, H. Jiang and Y. Li, *Green Chem.*, 2014, **16**, 3978–3985.
39 R. A. Maia, F. Berg, V. Ritleng, B. Louis and P. M. Esteves, *Chem.–Eur. J.*, 2020, **26**, 2051–2059.
40 M. Mu, Y. Wang, Y. Qin, X. Yan, Y. Li and L. Chen, *ACS Appl. Mater. Interfaces*, 2017, **9**, 22856–22863.
41 C. Qian, W. Zhou, J. Qiao, D. Wang, X. Li, W. L. Teo, X. Shi, H. Wu, J. Di, H. Wang, G. Liu, L. Gu, J. Liu, L. Feng, Y. Liu, S. Y. Quek, K. P. Loh and Y. Zhao, *J. Am. Chem. Soc.*, 2020, **142**, 18138–18149.
42 W. Leng, Y. Peng, J. Zhang, H. Lu, X. Feng, R. Ge, B. Dong, B. Wang, X. Hu and Y. Gao, *Chem.–Eur. J.*, 2016, **22**, 9087–9091.
43 W. Leng, R. Ge, B. Dong, C. Wang and Y. Gao, *RSC Adv.*, 2016, **6**, 37403–37406.
44 S. Kandambeth, D. B. Shinde, M. K. Panda, B. Lukose, T. Heine and R. Banerjee, *Angew. Chem., Int. Ed.*, 2013, **52**, 13052–13056.
45 A. Nagai, Z. Guo, X. Feng, S. Jin, X. Chen, X. Ding and D. Jiang, *Nat. Commun.*, 2011, **2**, 536–544.
46 X. Chen, M. Addicoat, S. Irle, A. Nagai and D. Jiang, *J. Am. Chem. Soc.*, 2013, **135**, 546–549.
47 B. Dong, L. Wang, S. Zhao, R. Ge, X. Song, Y. Wang and Y. Gao, *Chem. Commun.*, 2016, **52**, 7082–7085.
48 P. Y. Wang, M. M. Kang, S. Sun, Q. Liu, Z. H. Zhang and S. M. Fang, *Chin. J. Chem.*, 2014, **32**, 838–843.
49 R. N. Mozhchil, A. P. Menushenkov, A. M. Ionov, A. F. Mironov and V. D. Rumyantseva, *Macroheterocycles*, 2015, **8**, 252–258.
50 X. Kan, J. C. Wang, J. L. Kan, J. Y. Shang, H. Qiao and Y. B. Dong, *Inorg. Chem.*, 2021, **60**, 3393–3400.
51 J. Q. Zhang, Y. S. Peng, W. G. Leng, Y. A. Gao, F. F. Xu and J. L. Chai, *Chin. J. Catal.*, 2016, **37**, 468–475.
52 S. Ding, J. Gao, Q. Wang, Y. Zhang, W. Song, C. Su and W. Wang, *J. Am. Chem. Soc.*, 2011, **133**, 19816–19822.
53 M. Fan, W. Wang, X. Wang, Y. Zhu and Z. Dong, *Ind. Eng. Chem. Res.*, 2020, **59**, 12677–12685.
54 S. Asadi, R. Sedghi and M. Heravi, *Catal. Lett.*, 2017, **147**, 2045–2056.
55 J. Wang, C. Liu, X. Kan, X. Wu, J. Kan and Y. Dong, *Green Chem.*, 2020, **22**, 1150–1155.
56 A. Dhakshinamoorthy, M. Alvaro and H. Garcia, *ACS Catal.*, 2011, **1**, 48–53.
57 C. Meng, K. Yang, X. Fu and R. Yuan, *ACS Catal.*, 2015, **5**, 3760–3766.